Charged States of Four Isomers of C84 Fullerene: In Situ ESR and Vis−NIR Spectroelectrochemistry and DFT Calculations

ARTICLE *in* THE JOURNAL OF PHYSICAL CHEMISTRY C · APRIL 2009

Impact Factor: 4.77 · DOI: 10.1021/jp811274g

4 AUTHORS, INCLUDING:

Michal Zalibera
Max Planck Institute for Chemical Energy C…
30 PUBLICATIONS **274** CITATIONS
SEE PROFILE

Alexey A Popov
Leibniz Institute for Solid State and Materi…
188 PUBLICATIONS **3,410** CITATIONS
SEE PROFILE

Charged States of Four Isomers of C_{84} Fullerene: In Situ ESR and Vis−NIR Spectroelectrochemistry and DFT Calculations

Michal Zalibera,[†,‡] Peter Rapta,[†,‡] Alexey A. Popov,[†,§] and Lothar Dunsch*[,†]

Group of Electrochemistry and Conducting Polymers, Leibniz-Institute for Solid State and Materials Research Dresden, D-01171 Dresden, Germany, Department of Physical Chemistry, Faculty of Chemical and Food Technology, Slovak University of Technology, Radlinskeho 9, SK-81237 Bratislava, Slovak Republic, and Chemistry Department, Moscow State University, Moscow 119992, Russia

Received: December 20, 2008

An extended study of the spectroscopic and redox properties of four C_{84} fullerene isomers, C_{84}-C_2(11), C_{84}-C_s(14), C_{84}-D_2(22), and C_{84}-D_{2d}(23), is presented. The charged states of the C_{84} isomers are studied in detail by cyclic voltammetry and in situ spectroelectrochemistry. The anionic species of C_{84}, with the charge ranging from monoanion to tetraanion, are successively generated in *o*-dichlorobenzene solution at room temperature. Spectroscopic data include visible−near-infrared absorption spectra of all negatively charged states of C_{84} isomers as well as electron spin resonance spectra of C_{84}^- and C_{84}^{3-} paramagnetic fullerene ions. Cage isomers exhibit substantial differences in electronic structure. Consequently, different optical spectra of the neutral and charged forms of the C_{84} isomers are exhibited here, as well as in the ^{13}C splitting in the electron spin resonance (ESR) spectra. These findings are further supported by density functional theory (DFT) calculations of the spin density distribution and ESR spectra and time-dependent DFT calculations of the absorption spectra of the anionic species. Detailed interpretation of the experimental spectra is provided.

Introduction

The main limitation in the detailed knowledge of the redox and spectroscopic properties of higher fullerenes in different charged states is their low yield in synthesis. The limited quantities of isomerically pure material cause strong limitations in any study. Recently, we succeeded in isolating a large variety of higher fullerene isomers in their isomerically pure form (mostly C_{82} and C_{84} cages). The C_{84} fullerene is the third most abundant empty cage structure extractable from arc-processed soot. Its chemistry and electrochemistry was therefore studied in the past by many authors.[1−4] However, because of complications in the separation of individual isomers, most of the early studies were performed on isomeric mixtures. Among the 24 cages of C_{84},[5] only a few isomeric C_{84} structures were found to be stable enough to be isolated from the fullerene soot.[6−9] It is generally agreed that the C_{84} fraction of the fullerene soot consists mainly of two major isomers, namely, C_{84}-D_2(22) and C_{84}-D_{2d}(23), which occur in a roughly 2:1 ratio.[7,10,11]

At present, there have been few reports on the electrochemical and spectroscopic characterization of charged C_{84} fullerenes because of the very limited availability of purified C_{84} isomers.[1,12,13] Electron spin resonance (ESR) and visible−near-infrared (vis−NIR) studies of the charged C_{84} cages are quite rare and there is no systematic investigation of the negatively charged states of these cages at all. Because the ESR and vis−NIR spectra of charged fullerenes are of high importance in the characterization of the electronic state of fulleride anions,[14] this study focuses on a detailed characterization of the charged states of the C_{84} fullerene isomers in their isomeric pure state. In situ ESR and vis−NIR spectroelectrochemistry were the methods of choice used to achieve this goal. Very recently, we demonstrated for the C_{84}-D_{2d}(23) fullerene isomer that in situ ESR spectroelectrochemistry gives a clear insight into the isomeric purity of higher fullerenes and allows the detection of minor impurities whose presence is not found by other spectroscopic techniques.[15] Here, we report the electrochemical and spectroelectrochemical characterizations of the charged states of four C_{84} fullerene isomers, namely, C_{84}-C_2(11), C_{84}-C_s(14), C_{84}-D_2(22), and C_{84}-D_{2d}(23), to give new insights into the electronic state of the C_{84} fullerenes with respect to the stability of the cage isomers in endohedral fullerenes, where the charge contributes to the stability of the endohedral structure.

Experimental and Computational Details

The C_{84} isomers have been purified by an extended procedure reported in detail earlier.[15] The purity of the C_{84} samples was checked by ^{13}C NMR and matrix-assisted laser desorption ionization time-of-flight mass spectrometry (MALDI-TOF MS) measurements, and the results are given in the Supporting Information. For a typical electrochemical and spectroelectrochemical study, the solution of the C_{84} isomer in CS_2 was dried and placed into a glovebox, where it was immediately dissolved in *o*-dichlorobenzene (*o*-DCB, anhydrous, 99%, Aldrich, 2-fold vacuum distilled before use). The concentration of the fullerene in *o*-DCB ranged from 0.1 to 0.5 g L^{-1} ($1-5 \times 10^{-4}$ mol L^{-1}). Tetrabutylammonium hexafluorophosphate ($TBAPF_6$, Fluka, dried under reduced pressure at 340 K for 24 h prior to use) was used as the supporting electrolyte at a concentration of 0.2 mol L^{-1}. The cyclic voltammograms were obtained with a PAR 273 potentiostat (EG&G, USA) in a three-electrode system using platinum wires as working and counter electrodes and a silver wire as the pseudoreference electrode. Ferrocene (Fc) was added as the internal standard. A PG 284 potentiostat (HEKA, Germany) was used in the in situ ESR spectroelectrochemical studies. The ESR spectra were recorded with both Elexsys and

* To whom correspondence should be addressed. E-mail: l.dunsch@ifw-dresden.de.
† Leibniz-Institute for Solid State and Materials Research Dresden.
‡ Slovak University of Technology.
§ Moscow State University.

10.1021/jp811274g CCC: $40.75
Published on Web 03/10/2009

TABLE 1: Redox Potentials of C_{84} Isomers in Different Solvents

isomer	solvent/electrolyte	redox potential (V vs Fc/Fc^+)						$\Delta E_{gap,ec}$ (V)
		$E_{1/2,ox(1)}$	$E_{1/2,red(1)}$	$E_{1/2,red(2)}$	$E_{1/2,red(3)}$	$E_{1/2,red(4)}$	$E_{1/2,red(5)}$	
C_{84}-C_s(14)	*o*-DCB/ $TBAPF_6$	0.86	−0.78	−1.08	−1.60	−1.98	−	1.64
	BN/PPNCl [a]	−	−0.43	−0.76	−	−	−	−
	TCE/$TBAPF_6$ [a]	0.86	−0.77	−	−	−	−	1.63
C_{84}-C_2(11)	*o*-DCB/ $TBAPF_6$	0.85	−0.58	−0.87	−1.63	−1.97	−	1.43
	BN/PPNCl [a]	−	−0.28	−0.63	−1.46	−	−	−
	TCE/$TBAPF_6$ [a]	0.88	−0.59	−0.90	−	−	−	1.47
C_{84}-D_2(22)	*o*-DCB/ $TBAPF_6$	0.93	−0.79	−1.10	−1.40	−1.75	−	1.72
	BN/PPNCl [a]	−	−0.60	−0.96	−1.37	−1.60	−1.77	−
	TCE/$TBAPF_6$ [a]	−	−0.78	−1.06	−	−	−	−
	Py/$TBAClO_4$ [b]	−	−0.65	−0.98	−1.34	−1.75	−	−
C_{84}-D_{2d}(23)	*o*-DCB/ $TBAPF_6$	0.95	−0.77	−1.07	−1.36	−1.70	−	1.72
	BN/PPNCl [a]	−	−0.61	−0.96	−1.33	−1.63	−	−
	TCE/$TBAPF_6$ [a]	−	−0.79	−1.10	−	−	−	−
	Py/$TBAClO_4$ [b]	−	−0.46	−0.77	−1.58	−1.98	−2.27	−

[a] Potentials are taken from ref 12. [b] Potentials are taken from ref 13.

EMX X-band ESR spectrometers (Bruker, Germany), and the optical spectra were recorded with ultraviolet (UV)−vis and NIR spectrometer TIDAS systems (J&M, Aalen, Germany).

Optimization of geometric parameters was performed using a PBE functional[16] and TZ2P quality basis set with a {6,3,2}/(11s,6p,2d) contractation scheme implemented in the PRIRODA package.[17,18] The code employed expansion of the electron density in an auxiliary basis set to accelerate evaluation of the Coulomb and exchange−correlation terms.[17] PRIRODA and PBE were also employed in time-dependent density functional theory (TD-DFT) calculations. However, an increase in the number of excited states being studied resulted in a drastic increase in computational demands; therefore, calculations were performed using the modest basis set of double-ζ (DZ) quality. Preliminary calculations with the TZ2P basis and a reduced number of excited states showed that the use of the smaller basis set did not result in qualitative changes of the predicted spectra. Point energy calculations of the spin density distribution in C_{84}^- radical anions with the hybrid B3LYP functional and the EPR-II basis set[19] were performed with the use of the PC GAMESS package.[20]

Results and Discussion

Cyclic Voltammetry. Before starting detailed in situ spectroelectrochemical experiments, we performed standard cyclovoltammetric studies of all four C_{84} isomers in order to monitor the redox behavior with the supporting electrolyte used for the ESR and vis−NIR cyclovoltammetric studies. Figure 1 shows the cyclic voltammograms of C_{84}-C_2(11), C_{84}-C_s(14), C_{84}-D_2(22), and C_{84}-D_{2d}(23) in an *o*-DCB/$TBAPF_6$ solution. Four reversible reduction steps and one oxidation step were detected for all samples in the potential window available. Electrochemical data evaluated from the cyclic voltammetry of the investigated C_{84} fullerene isomers are summarized in Table 1. Comparisons of the half-wave potentials in *o*-DCB to those measured in benzonitrile (BN) and 1,1,2,2-tetrachloroethane (TCE) from ref 12 and in pyridine (Py) from ref 13 are also given.

Authors of ref 12 reported two reduction peaks for the C_{84}-C_s(14) isomer in the BN/PPNCl {PPN = $[(C_6H_5)_3P]_2N^+$} system and one oxidation and one reduction peak using a TCE/$TBAPF_6$ solvent/supporting electrolyte combination. The first and second reduction half-wave potentials ($E_{1/2}$) are negatively shifted in *o*-DCB compared to those in BN, similar to those observed in TCE. However, the half-wave potentials of the first reduction and oxidation in *o*-DCB as well as the electrochemical energy gap ($\Delta E_{gap,ec}$) are almost identical with those found in TCE. A strong positive shift of the reduction potentials is found for the BN/PPNCl system compared to those of the *o*-DCB/$TBAPF_6$ solutions, and almost the same values are detected in *o*-DCB and TCE for isomer C_{84}-C_2(11) (Table 1). It should be mentioned that the reduction of C_{84}-C_s(14) as well as that of the C_{84}-C_2(11) isomers to the trianion and tetraanion is observed in *o*-DCB and is reported in this study for the first time (Figure 1a,b). Both $E_{1/2}$ values for the third and fourth reduction peaks for the C_{84}-C_2(11) isomer are more negatively shifted compared to those of isomer C_{84}-C_s(14). Consequently, the potential difference between the second and third reduction peaks is about 240 mV larger in the case of C_{84}-C_2(11).

Cyclic voltammetry of isomer C_{84}-D_2(22) shows four reversible reduction steps and one oxidation step in *o*-DCB/$TBAPF_6$ (Figure 1c), similar to that of the other C_{84} isomers. However, in this case the reduction steps are almost equally spaced, and no potential gap is observed between the second and third reduction peaks as opposed to the findings for the isomers with lower symmetry. In this way, the voltammetry of the C_{84}-D_2(22) isomer resembles that of Buckminster fullerene C_{60}. Figure 1d shows the cyclic voltammetry of C_{84}-D_{2d}(23). In this case, the spacing between the reduction steps is almost equal, similar to that of C_{84}-D_2(22). In fact, the C_{84}-D_2(22) and C_{84}-D_{2d}(23) isomers have redox potentials quite close to each other, and distinguishing between them in a mixture just on the basis of the voltammetric experiment is quite complicated. The half-wave ($E_{1/2}$) potentials recorded are −0.77, −1.07, −1.36, and −1.70 V versus Fc/Fc^+ for the four reductions and 0.95 V versus Fc/Fc^+ for the first oxidation step. Azamar-Barrios et al. have reported the cyclic voltammetry of the C_{84}-D_{2d}(23) fullerene in benzonitrile (BN) and 1,1,2,2-tetrachloroethane (TCE).[12] The $E_{1/2}$ values for the reduction steps in BN are positively shifted with respect to those of *o*-DCB, but those in the TCE are almost identical.[12] Neither our measurements nor other literature data confirm significant differences between the second and third reduction potentials of C_{84}-D_{2d}(23) reported by Anderson et al.[13] A small impurity peak was observed in the anodic part of the voltammogram similar to that of C_{84}-D_2(22) (marked with an asterisk in Figure 1c,d) and was recently attributed to the small amount of the C_{82}-C_2(3) isomer applied during in situ ESR and vis−NIR spectroelectrochemical studies.[15]

Spectroelectrochemistry. ***I. Monoanions and Dianions.*** The first spectroelectrochemical studies were focused on ESR and optical spectra of monocharged C_{84} isomers. Figure 2 shows

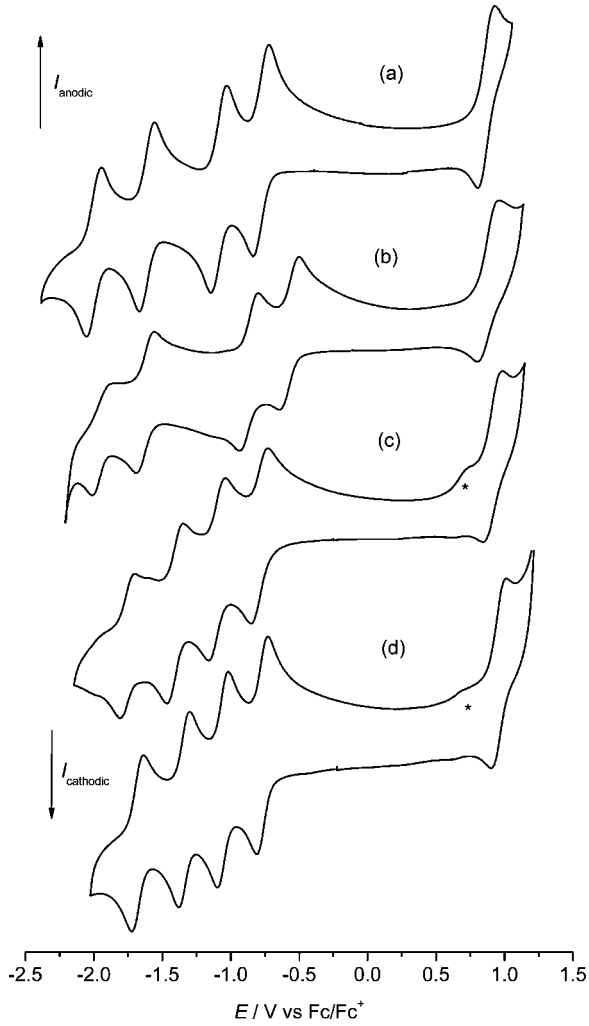

Figure 1. Cyclic voltammetry of (a) C_{84}-C_s(14), (b) C_{84}-C_2(11), (c) C_{84}-D_2(22), and (d) C_{84}-D_{2d}(23) isomers at room temperature in 0.2 M $TBAPF_6$/*o*-DCB; sweep rate = 100 mV s^{-1}; * in (c and d) marks the C_{82}-C_2(3) impurity peak.

the spectroelectrochemical response observed in the range of the first electron transfers in the cathodic part for all studied C_{84} isomers as illustrated for the reduction of isomer C_{84}-C_2(11) in an *o*-DCB/$TBAPF_6$ solution. In Figure 2, the time course of the ESR spectra detected during the in situ spectroelectrochemistry of C_{84}-C_2(11) in the range of the first reduction peak is presented. A sharp ESR line (ΔB_{pp} = 0.19 G) at g = 2.0004 (Figure 3b) rises and decreases in the ESR spectra following the potential sweep. This signal can be clearly assigned to the monoanion of the C_{84}-C_2(11) isomer. Simultaneously, during the in situ ESR and vis−NIR cyclovoltammetry of C_{84}-C_2(11) in the potential range of the first reduction step, new optical bands with maxima at 860, 1180, 1420, and 1770 nm arise (Figure 4b, red line), and because of the correlation of their intensities with the intensity of the ESR line, they can be assigned to the monoanion of C_{84}-C_2(11). A similar behavior was observed for the other three C_{84} isomers under study with a different pattern of optical bands of monoanions, depending on the C_{84} fullerene structure. ESR as well as optical spectra of the radical anions of all investigated C_{84} isomers are summarized in Figures 3 and 4, respectively.

For the lower symmetric isomers, C_{84}-C_s(14) and C_{84}-C_2(11), sharp singlet ESR lines accompanied by ^{13}C satellites [ΔB_{pp} = 0.20 G and g = 2.0011 for C_{84}-C_s(14)] were monitored (Figure 3a,b). A similar sharp and intense ESR signal with a ^{13}C satellite

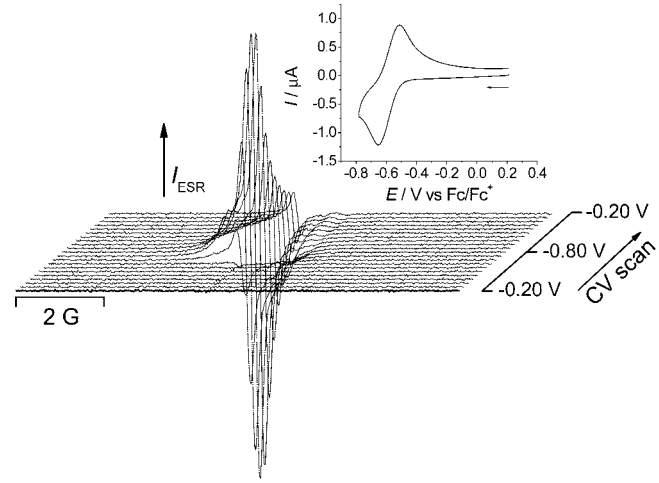

Figure 2. Time course of ESR spectra detected during the cyclic voltammetry of C_{84}-C_2(11) in the potential region of the first reduction step. Inset shows the corresponding cyclic voltammogram (0.2 M $TBAPF_6$/*o*-DCB, scan rate = 3 mV s^{-1}).

pattern was recently reported by our group for the monoanion and monocation of the main isomer of the C_{82} fullerene with C_2 symmetry.[21] The ESR spectrum of the C_{84}-C_s(14) isomer monoanion was already reported in ref 12 with a g value for the frozen solution (4 K) of 2.0012, which is very close to the value reported here. However, for the defrosted solution, a three-line ESR spectrum was reported in ref 12. The most intense line has approximately the same line width as observed in our case, but the two surrounding lines were not observed in our experiments with the highly purified sample. So, the presence of some paramagnetic impurities in the sample used in ref 12 should be assumed.

The C_{84}-D_2(22) isomer exhibits a sharp but not very intense line (g = 2.0008, ΔB_{pp} = 0.17 G) as shown in Figure 3c. Some sidebands were also observed, but the line shape was slightly asymmetric for the main signal. In the high-performance liquid chromatography (HPLC) setting used in this work, the C_{82}-C_2(3) fraction is preceding and partially overlapping the C_{84}-D_2(22) fraction. It is possible that the asymmetry of the ESR signal is caused by trace amounts of C_{82}-C_2(3) present in the C_{84}-D_2(22) sample even after multiple-stage recycling HPLC treatment because its monoanion signal has a very close g factor of 2.0009,[21] and a small signal of C_{82} was detected in our sample by mass spectrometry.

Reduction of the C_{84}-D_{2d}(23) isomer in the potential region of the first reduction step resulted in a quite complicated ESR spectrum, consisting of at least three signals (Figure 3d). Recently, the monoanion of a purified C_{84}-D_{2d}(23) fullerene isomer was studied by ESR spectroelectrochemistry in detail.[15] The main relatively broad signal with a g factor of 2.0013 and a line width of ΔB_{pp} = 1.00 G was unambiguously attributed to a C_{84}-D_{2d}(23) monoanion. The minor impurity in the C_{84} monoanion ESR spectrum, with a sharp line (ΔB_{pp} = 0.15 G) and g factor of 2.0009, which comprises 2% of the signal, was identified as a monoanion of the C_{82}-C_2(3) isomer. The second impurity in C_{84}-D_{2d}(23) is attributed to the C_{84}-C_s(16) isomer as these two isomers of C_{84} have very close retention times.[6]

Summarizing the ESR results of the C_{84} fullerene monoanions, we conclude that the symmetry of the fullerene molecule has a strong influence on the line width of the ESR signal of the monoanion, which decreases by decreasing the cage symmetry, as is already reported for fullerene dimers.[22] A more detailed discussion explaining these observations is given in the section titled Structures of Anions and Spin Density Distribution.

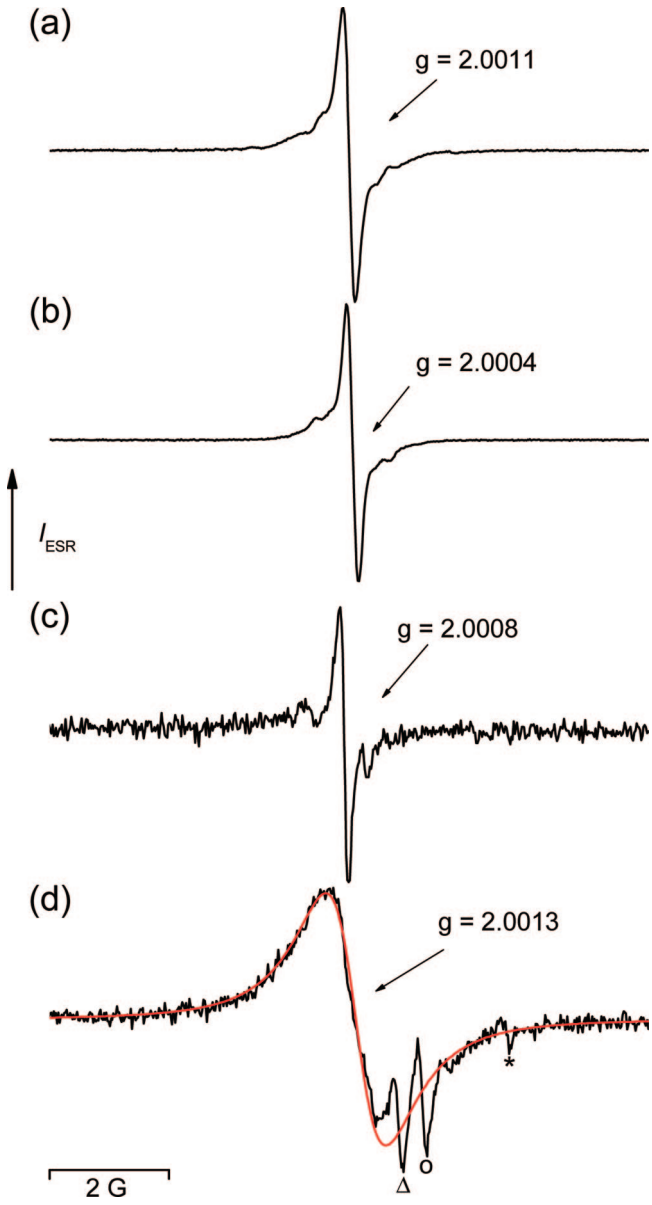

Figure 3. ESR spectra of anion radicals of the (a) C_{84}-C_s(14), (b) C_{84}-C_2(11), (c) C_{84}-D_2(22), and (d) C_{84}-D_{2d}(23) isomers detected in the potential region of the first reduction step at room temperature in 0.2 M $TBAPF_6$/*o*-DCB solutions; △ marks C_{82}-C_2(3), ○ marks C_{84}-C_s(16), and * marks an unknown impurity.

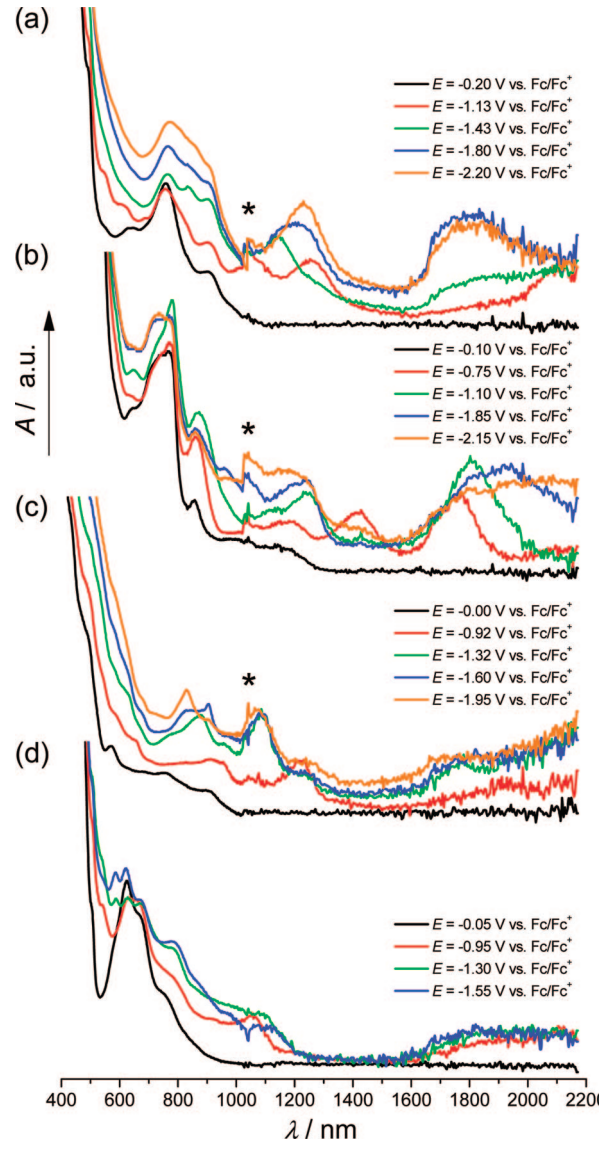

Figure 4. Vis−NIR spectra of neutral fullerenes (black), monoanions (red), dianions (green), trianions (blue), and tetraanions (orange) of the (a) C_{84}-C_s(14), (b) C_{84}-C_2(11), (c) C_{84}-D_2(22), and (d) C_{84}-D_{2d}(23) isomers detected at room temperature in 0.2 M $TBAPF_6$/*o*-DCB solutions; * marks spectrometer artifacts.

Cage isomers of the same fullerene size usually exhibit substantial differences in their electronic structure and, consequently, also in the optical spectra of the neutral and charged states. Thus, the first reduction of C_{84}-C_s(14) was related to the new optical bands with maxima at 548, 1048, and 1261 nm and a broader one with a maximum around 2110 nm (Figure 4a, red line). These features are completely different from those at 860, 1180, 1420, and 1770 nm observed for isomer C_{84}-C_2(11) (Figure 4b, red line). For isomer C_{84}-D_2(22), new bands at 653, 912, and 1222 nm and a broader one with a maximum around 1910 nm were monitored (Figure 4c, red line). For isomer C_{84}-D_{2d}(23), new optical bands with maxima at 540, 1054, and 2110 nm occurred at the first reduction peak (Figure 4d, red line). Their intensities correlate well with the intensity of the broader ESR signal during the in situ spectroelectrochemical experiment, and consequently, these spectral features can be reliably assigned to the same species, namely, the monoanion of C_{84}-D_{2d}(23). Simultaneously, a decrease in the optical band of neutral C_{84}-D_{2d}(23) at 625 nm was observed.

When the potential range was expanded to the second reduction step, a decrease in the intensity of the monoanion ESR line was observed for all isomers as illustrated for the C_{84}-C_s(14) isomer in Figure 5a. This experiment confirms the diamagnetic character of the dianion formed upon reduction. During the back scan, the intensity of the ESR signal increases after the reoxidation of the dianion to the monoanion. The nonzero intensity of the ESR signal at the potentials of the second reduction step can be easily explained by the synproportionation reaction, which obviously occurs in the bulk solution in the potential region of the second electron transfer and by the diffusion of the radical anion into the bulk solution, where it is still detectable by ESR. New optical bands with maxima at 835, 1147, and around 1850 nm occurred in the vis−NIR spectra when extending the potential sweep to the second reduction step (Figures 4a and 5b, green lines). These bands can be again assigned to the C_{84}-C_s(14) dianion because of the correlation

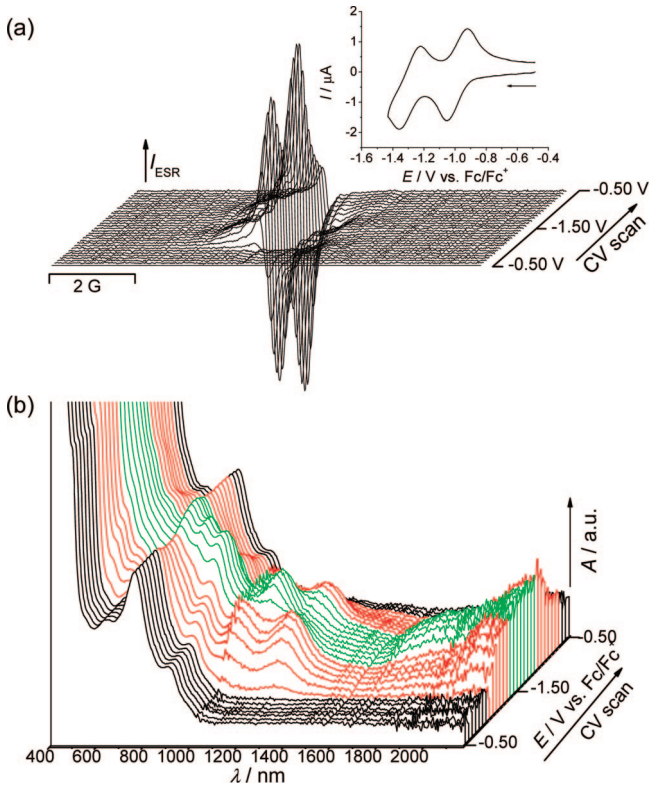

Figure 5. (a) Time course of the ESR spectra detected during the cyclic voltammetry of C_{84}-C_s(14) in the potential region of the first and second reduction step. Inset figure shows the corresponding voltammogram (0.2 M $TBAPF_6$/*o*-DCB, scan rate = 3 mV s^{-1}). (b) Vis−NIR spectra observed during the cyclic voltammetry of C_{84}-C_s(14) in the potential region of the first and second reduction step (neutral, black lines; monoanion, red lines; dianion, green lines).

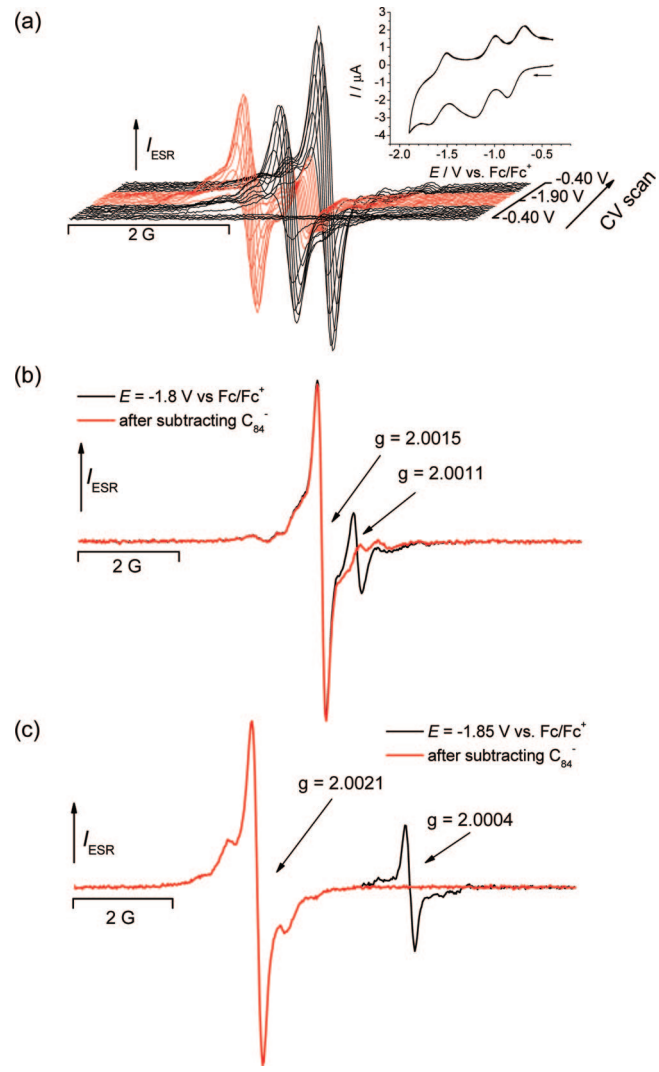

Figure 6. (a) Potential dependence of the ESR spectra of C_{84}^{-}-C_s(14) and C_{84}^{3-}-C_s(14) in the potential region of the first, second, and third reduction step. The inset shows the corresponding cyclic voltammogram (0.2 M $TBAPF_6$/*o*-DCB, scan rate = 4.5 mV s^{-1}). (b) ESR spectrum of C_{84}^{3-}-C_s(14) overlapped by the signal of C_{84}^{-}-C_s(14) (black line) and after C_{84}^{-}-C_s(14) signal subtraction (red line). (c) ESR spectrum of C_{84}^{3-}-C_2(11) with the signal of C_{84}^{-}-C_2(11) (black line) and after C_{84}^{-}-C_2(11) signal subtraction (red line).

of their intensities with the charge transferred in the second reduction step.

Three new optical bands with maxima at 780, 1240, and 1805 nm, which can be assigned to the C_{84}-C_2(11) dianion, were detected during the reduction of the C_{84}-C_2(11) isomer at the second reduction peak (Figure 4b, green line). Additionally, a decrease in the intensity of the monoanion band at 1420 nm was observed. New optical bands at 870, 1085, and 1780 nm and one probably beyond the limit of the detector (>2175 nm) were observed for the C_{84}-D_2(22) reduction at the second reduction peak and can be tentatively assigned to the C_{84}-D_2(22) dianion (Figure 4c, green line). Additionally, the monoanion band at 1222 nm decreased during the reduction of C_{84}-D_2(22) to the dianionic state and increased after reoxidation. Reduction of isomer C_{84}-D_{2d}(23) in the potential region of the second reduction step leads to the appearance of new bands at 586, 785, 1095, and 1905 nm, which can be ascribed to the C_{84}-D_{2d}(23) dianion on the basis of the correlation of their intensities with cyclic voltammetry (Figure 4d, green line).

II. Trianions and Tetraanions. During reduction of the C_{84}-C_s(14) isomer at the third reduction step, a new ESR signal appeared with a *g* factor of 2.0015 and a line width of ΔB_{pp} = 0.18 G (Figure 6a). This new signal can be assigned to the C_{84}-C_s(14) trianion, according to the correlation of its intensity with the third reduction and reoxidation peaks in the cyclovoltammetric trace. Because there were some monoanion species diffused in the bulk solution, the new ESR signal was partially overlapped by a monoanion line. However, subtraction of the monoanion signal was easily possible, which resulted in the ESR spectrum of the C_{84}-C_s(14) trianion dominated by a single sharp line similar to that of the monoanion signal but with a different ^{13}C satellite pattern (Figure 6b). Because of the low symmetry, Jahn−Teller distortion is not expected for the C_{84}-C_s(14) isomer in the charged state, and C_s is expected for all charged states of this isomer. In such a situation, the spin density in the monoanion and trianion reflects the lowest unoccupied molecular orbital (LUMO) and LUMO+1 orbital densities, respectively, of the neutral molecule, and hence, the ^{13}C patterns are different for the C_{84} monoanions and C_{84} trianions. The increase in the intensity of the two absorption bands at 1208 and 1780 nm was observed in the vis−NIR spectra at the potentials of the third reduction step for C_{84}-C_s(14) (Figure 4a, blue line). Intensity of the dianion band at 1147 nm decreased at these potentials. The intensities of both bands correlate well with the changes in the ESR spectra of the C_{84}-C_s(14) trianion. Moving to even more negative potentials, including the fourth reduction step of C_{84}-C_s(14), we observed a decrease of the trianion ESR signal, and no new ESR signals occurred, showing that similar to the dianion the tetraanion of the C_{84}-C_s(14) fullerene is diamagnetic.

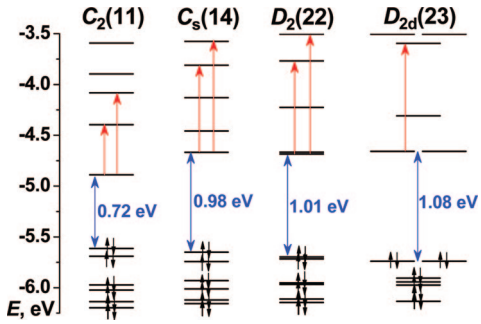

Figure 7. MO levels in the $C_2(11)$, $C_s(14)$, $D_2(22)$, and $D_{2d}(23)$ isomers of C_{84} computed at the PBE/TZ2P level. Vertical red arrows schematically denote the highest-intensity excitations of the anions.

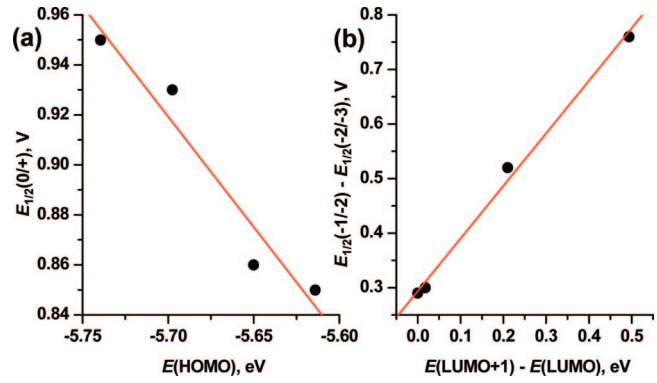

Figure 8. Correlation between (a) HOMO energy and the first oxidation potential and (b) LUMO−LUMO+1 gap and the difference between the second and third reduction potentials of the C_{84} isomer. MO energies are computed at the PBE/TZ2P level of theory.

The vis−NIR spectrum of the tetraanion is presented (Figure 4a, orange line).

In the case of isomer C_{84}-$C_2(11)$, a new well-defined ESR line with a shifted g value (g = 2.0021, ΔB_{pp} = 0.19 G) appeared at the third reduction peak. Simultaneously, the ESR line of the monoanion decreased continuously. A larger separation in g factors between the signals of the monoanion and trianion was observed compared to that of the C_{84}-$C_2(11)$ isomer, and again the ^{13}C satellite patterns are different for the singly and triply charged fullerene (Figure 6c). The vis−NIR spectra at the third reduction of the C_{84}-$C_2(11)$ isomer are accompanied by a rise of additional bands at 734, 960, and 1930 nm (Figure 4b, blue line). Simultaneously, a decrease in the intensity of the dianion band at 1805 nm is observed.

For isomer C_{84}-$D_2(22)$, the reduction at potentials of the third step was followed by a rise of bands at 832 and 903 nm and a maximum of the dianion band around 1780 nm shifted to approximately 1820 nm. Therefore, the bands at 832 and 903 nm can be tentatively assigned to the trianion of C_{84}-$D_2(22)$ (Figure 4c, blue line). Unfortunately, in the ESR spectra, no signal was found that could be unambiguously assigned to C_{84}^{3-}-$D_2(22)$. Surprisingly, during the reduction in the potential range of the fourth step, a new ESR line with a g factor of 2.0019 appeared and vanished after reoxidation. As the C_{82} trianion shows an ESR signal at the same g factor,[23] this new signal can be assigned to these species because the third reduction peak of C_{82} would partially overlap the fourth reduction of C_{84}-$D_2(22)$. In the vis−NIR spectra, a new band at 829 nm appeared, and the C_{84}^{3-}-$D_2(22)$ band at 903 nm decreased during reduction at the potentials around the fourth step (Figure 4c, orange line).

Moving to the third reduction peak, we expected the rise of a new ESR signal for the trianion of the C_{84}-$D_{2d}(23)$ isomer. Unfortunately, no new distinct signal was detected. However, changes in the shape of the ESR line ascribed to the monoanion allow us to speculate that the trianion has a similar g factor as the monoanion, and as some of the monoanion was already diffused into the bulk solution in this phase of experiment, an overlap of these two signals was observed. In the vis−NIR spectra, no dramatic change was observed during reduction at potentials of the third step, and the same is valid also for the experiment, where the fourth reduction step was included in the cyclic voltammetry (Figure 4d, blue and orange lines).

Theoretical Calculations of Frontier Molecular Orbital (MO) Levels. To rationalize the observed data, we have performed a series of DFT calculations of the molecular structures and electronic spectra of the C_{84} isomers in the neutral and charged forms. Figure 7a shows the energy levels of the frontier molecular orbitals for the four isomers in their neutral state. HOMO energy decreases in row $C_2(11)$−$C_s(14)$−$D_2(22)$−$D_{2d}(23)$, and these data reasonably correlate to the oxidation potentials measured for these isomers (see Figure 8a for the correlation). $C_s(14)$, $D_2(22)$, and $D_{2d}(23)$ isomers have virtually the same LUMO energy, which results in almost identical first reduction potentials observed experimentally. At the same time, the LUMO of $C_2(11)$ is considerably lower in energy, and it agrees with its anodically shifted reduction potential. In general, these results agree well with the data reported earlier on MO levels and reduction potentials by Azamar-Barrios et al.[12]

The difference between the second and third reduction potentials corresponds to the gap between LUMO and LUMO+1. Indeed, calculations show that the largest LUMO−LUMO+1 gap is found for the $C_2(11)$ isomer (0.49 eV), followed by the $C_s(14)$ isomer with a value of 0.21 eV, while for the $D_2(22)$ and $D_{2d}(23)$ isomers these gaps are negligible. For the $D_{2d}(23)$ isomer, the gap is exactly zero because the LUMO has E symmetry and is 2-fold degenerated, while for the $D_2(22)$ isomer the quasidegeneracy of LUMO and LUMO+1 within 0.02 eV is accidental but can be also related to the close similarity of the structures of $D_2(22)$ and $D_{2d}(23)$ isomers. The orbital gaps perfectly correspond to the measured difference of the second and third reduction potentials (Figure 8b).

Structures of the Anions and Spin Density Distribution. The optimization of the structures of the anions was performed at the PBE/TZ2P level without symmetry constraints to ensure that any possible distortions of the symmetry due to electron transfer can be found in the calculations. Similar to the C_{82}-$C_2(3)$ isomer studied by us recently, the $C_2(11)$, $C_s(14)$, and $D_2(22)$ isomers are found to have the same symmetry in the anionic state as in their neutral states because these isomers have no degenerated MO levels and, hence, are not subjected to the Jahn−Teller effect. On the contrary, the degenerated LUMO of the $D_{2d}(23)$ isomer results in the Jahn−Teller distortion of the anionic states of this isomer. In particular, DFT calculations show that its symmetry is reduced to D_2. However, this distortion is not very strong, and the difference in the bond lengths that would be equivalent in a D_{2d} symmetric structure does not exceed 0.008 Å in the Jahn−Teller-distorted monoanion. The HOMO−LUMO gap of the dianion, i.e., the gap between the orbitals originating from the double-degenerated LUMO of C_{84}-$D_{2d}(23)$, is only 0.03 eV.

In the detailed study of a series of C_{60} derivatives, Fukuzumi et al. have shown that the ESR linewidth of the anion radicals can be correlated to the gap between the singly occupied

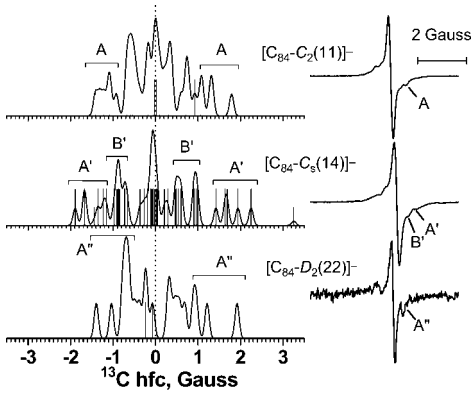

Figure 9. Distribution of $a(^{13}C)$ values in the anions of the $C_2(11)$, $C_s(14)$, and $D_2(22)$ isomers as computed at the B3LYP/ESR-II//PBE/TZ2P level (bars represent individual values and curves correspond to broadening with the Gaussian function with a half-width of 0.1 G). Right panel shows experimental ESR spectra and tentative assignment of experimental ^{13}C satellite features.

molecular orbital (SOMO) and two other orbitals originating from the t_{1u} MO of parent C_{60}, with narrow signals corresponding to large gaps and vice versa.[24] An analogous correlation can explain why the broadest ESR signal in this work is observed for the C_{84}-$D_{2d}(23)$ isomer with degenerated LUMO. In the monoanion, the gap between the SOMO and LUMO of the $D_{2d}(23)$ isomer is only 0.039 eV. A two-times larger value of 0.076 eV is predicted for the $D_2(22)$ isomer, while for $C_s(14)$ and $C_2(11)$ the gaps are as high as 0.289 and 0.545 eV, respectively. However, the gap in the $D_{2d}(23)$ isomer is comparable to that estimated for C_{60}^-, but the ESR signal of C_{84}^--$D_{2d}(23)$ is still much more narrow than that of C_{60}^-. The quasidegeneracy of LUMO and LUMO+1 in the $D_2(22)$ isomer could also result in the broadening of its ESR signal, which is not actually observed.

Figure 9 shows the distribution of the ^{13}C hyperfine-splitting constants in anion radicals computed at the B3LYP/EPR-II//PBE/TZ2P level. DFT-predicted $a(^{13}C)$ values fall in the range of $|a| < 2$ G, the only exclusion being C_{84}-$C_s(14)$, which has two atoms with large values (2.25 and 3.26 G). Dense distributions of the $a(^{13}C)$ values and relatively low molecular symmetry preclude a precise assignment of the experimental features to specific atoms, and only groups of values can be tentatively suggested as shown in Figure 9. A complete set of DFT-computed $a(^{13}C)$ hyperfine-splitting constants is available in the Supporting Information.

TD-DFT Calculations of Absorption Spectra. The reduction (occupation of the LUMO) of the fullerene is expected to result in two major groups of changes in the electronic absorption spectra: (a) disappearance of the former HOMO-N→LUMO excitations (because LUMO is not vacant any more) and (b) appearance of new excitations from the former LUMO (SOMO in the monoanion and HOMO in the dianion) to the higher-energy vacant MOs. The second group is responsible for the characteristic strong absorptions of the fullerene anions appearing in the near-infrared range (e.g., at 1080 nm in C_{60}^- and 940 nm in C_{60}^{2-}, see ref 14 for a review). Certainly, this description is oversimplified because not all excitations can be well-described by one configuration, and more complex changes in the spectra are actually expected. Moreover, for the monoanions, which have an open-shell electronic structure with SOMO, a superposition of $\alpha\rightarrow\alpha$ and $\beta\rightarrow\beta$ excitations with different energies is expected.

To interpret absorption spectra of the anionic states of the C_{84} isomers in more detail, we have performed TD-DFT calculations of their excitation energies and oscillator strengths. It is shown that TD-DFT (with GGA functionals) normally underestimates excitation energies of fullerenes, so the shift of the energy should be applied to match experimental data.[25,26] Bauernschmitt et al. reported that for the fullerenes the average shift of 0.36 eV for the whole energy range gives reasonable results.[25] In this work, we focus on the energy range below 2 eV, and it appears (Figure 10) that the shift of computed excitation energies by 0.2 eV results in perfect correspondence of the experimental and computed absorption spectra (note the shift of TD-PBE-computed excitation energies by 0.2 eV is also applicable for the lowest energy excitation in C_{60}, which occurs at around 1.9 eV[26]). At the same time, our testing calculations for C_{60}^- and C_{70}^- anions have shown that energies of characteristic NIR absorptions are predicted by TD-DFT very well without any energy shift. That is, TD-DFT has different systematic errors for the transitions of different natures, as was already demonstrated for polycyclic aromatic hydrocarbons (PAHs).[27] For C_{60}^- and C_{70}^-, this fact does not result in difficulties of the spectral assignment because these fullerenes have high HOMO−LUMO gaps in the neutral form, and new excitations of their anions are well-separated in energy from those that are analogous to excitations in neutral fullerenes. However, for the isomers of C_{84}, which have much lower HOMO−LUMO gaps, this shortcoming of TD-DFT results in serious problems in spectra interpretation because characteristic absorptions of anions overlap with the rest of the excitations. Hence, to provide a reliable assignment of spectra, first we have analyzed the nature of the excitations. Computed spectra (Figure 10) are color-coded to distinguish different types of excitations. Blue-colored lines are used to denote HOMO-N→LUMO excitations in neutral fullerenes and their analogs in the charged forms, while red-colored lines are used to denote SOMO→LUMO+N and HOMO→LUMO+N excitation of the monoanions and dianions, respectively. Plotting Figure 10, we applied a shift of +0.2 eV for the whole set of computed excitation energies, but on the basis of the discussion given above, we expect that for the red-coded excitations, the originally computed TD-DFT excitation energies are in better agreement with experimental data than after the energy shift. Once this fact is taken into account, the assignment of the spectra of the monoanions and dianions is straightforward. In the following discussion, we will denote the orbitals based on their nature in the neutral state to simplify correlation between excitations of the different charge states, e.g., "LUMO" denotes the LUMO orbital of neutral C_{84} as well as SOMO in C_{84}^- and HOMO in C_{84}^{2-}.

In anions of the $C_2(11)$ isomer, two major NIR transitions observed at 0.70 and 0.87 eV for the monoanion and at 0.69 and 1.00 eV for the dianion are assigned to the excitations corresponding to LUMO→LUMO+1 and LUMO→LUMO+2, respectively, in neutral C_{84} (Figure 7).

The LUMO−LUMO+1 gap of the $C_s(14)$ isomer is too small, and in its charged states the LUMO→LUMO+1 excitation appears at low energy and according to the TD-DFT calculations has a small intensity. Likewise, low transition intensity is also predicted for the excitation corresponding to the LUMO→LUMO+2 excitation, and they cannot be unambiguously assigned in the experimental spectrum. Therefore, transitions at 0.99 eV (monoanion) and 1.08 eV (dianion) in the spectra of the charged $C_s(14)$ isomer are unambiguously assigned to the LUMO→LUMO+3 excitation. Assignment of the LUMO→LUMO+4 excitation, which also falls in the energy range below 2 eV and has high

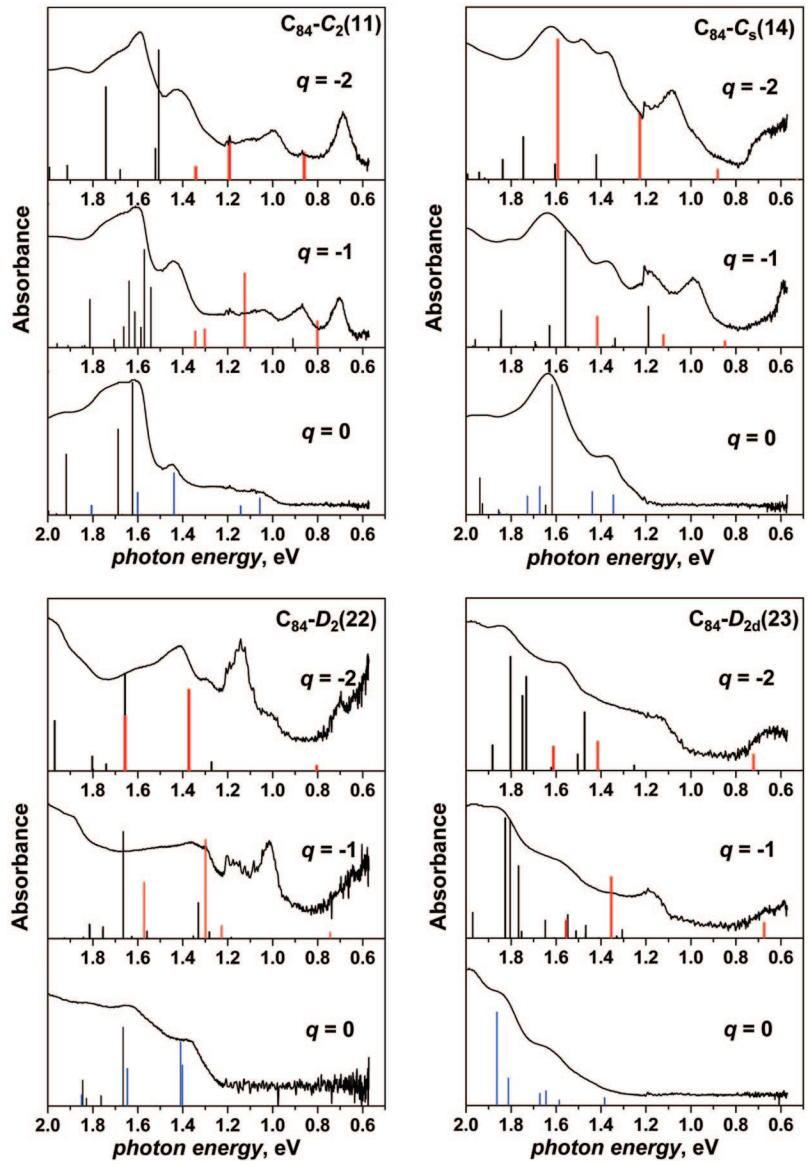

Figure 10. Experimental and TD-DFT-computed excitation spectra of $C_2(11)$, $C_s(14)$, $D_2(22)$, and $D_{2d}(23)$ isomers of C_{84} in the neutral, monoanionic, and dianionic forms in the range of 0.5−2.0 eV.

intensity, is more difficult because it overlaps with excitations having the same character as in neutral fullerene.

LUMO→LUMO+3 and LUMO→LUMO+4 excitations are most intense in anions of the $D_2(22)$ isomer. The former corresponds to the transitions observed at 1.02 eV (monoanion) and 1.14 eV (dianion). As to LUMO→LUMO+4, its energy falls in the range of HOMO→LUMO and HOMO-1→LUMO excitations of neutral C_{84}-$D_2(22)$ at around 1.4 eV, and in the spectrum of the monoanion, these excitations correspond to the broadband at 1.30−1.36 eV. In the spectrum of the dianion, all HOMO-N→LUMO excitations disappear, and the band at 1.41 eV is assigned presumably to the LUMO→LUMO+4 excitation.

The $D_{2d}(23)$ isomer has the highest HOMO−LUMO gap, its LUMO is 2-fold degenerate, and all excitations of neutral C_{84} in the <2 eV range are HOMO-N→LUMO in nature. As already discussed, LUMO of C_{84}-$D_{2d}(23)$ is split in anionic forms. As a result, many excitations of the HOMO-N→LUMO type are preserved in charged states, and the spectra of the monoanions and dianions are more similar to the spectrum of the neutral form than to those of other isomers. At the same time, specific NIR excitations of the C_{84}-$D_{2d}(23)$ anions can be better distinguished. Transitions at 1.18 eV (monoanion) and 1.13 eV (dianion) are assigned to the LUMO→LUMO+2 excitation. The LUMO→LUMO+1 transition has a lower intensity and can be tentatively assigned to the features appearing at 0.66 eV in the spectra of both anionic forms.

Conclusions

Special efforts were devoted to the generation and characterization of the charged states of four purified C_{84} isomers, C_{84}-$C_2(11)$, C_{84}-$C_s(14)$, C_{84}-$D_2(22)$, and C_{84}-$D_{2d}(23)$, in their neutral and negatively charged forms. In summary, the in situ ESR and vis−NIR spectroelectrochemistry was shown to be a powerful tool in the analysis of the charged isomeric structures of higher fullerenes. Spectroscopic data now available include vis−NIR absorption spectra of all negatively generated charged states of studied the C_{84} isomers as well as ESR spectra of C_{84}^- and C_{84}^{3-} paramagnetic fullerene ions. Cage isomers of the same fullerene usually exhibit substantial differences in their electronic structure, and consequently, different optical spectra of neutral and charged forms of the C_{84} isomers were observed. We have found remarkable differences in line widths as well as in ^{13}C

satellite patterns of the C_{84}^{-} and C_{84}^{3-} radicals. The monoanion of the C_{84} isomer with C_s symmetry exhibits a sharp ESR spectrum with $\Delta B_{pp} = 0.16$ G in contrast to the monoanion of the C_{84}-$D_{2d}(23)$ fullerene isomer with $\Delta B_{pp} = 1$ G. The radical anions of C_{60} and C_{70} exhibit broad ESR signals due to the degeneracy of their LUMOs in these fullerenes, so the same holds true for the $D_{2d}(23)$ isomers of C_{84}.

Acknowledgment. We cordially thank Ms. K. Leger, Ms. S. Schiemenz, and Mr. F. Ziegs for technical assistance. M.Z. and P.R. thank Alexander von Humboldt Foundation for financial support (Projekt 3 Fokoop DEU/1063827 with funds from the Federal Ministry for Education and Research). The support of SGA VEGA 1/0018/09 to P.R. is also acknowledged. A.P. thanks Alexander von Humboldt Foundation and Civilian Research and Development Foundation (RUC2-2830-MO-06) for financial support and U. Nitzsche for technical assistance related to computer resources at IFW.

Supporting Information Available: MS and NMR spectra of purified C_{84} isomers and a full list of DFT-computed $a(^{13}C)$ values for C_{84} monoanions and their Cartesian coordinates. This material is available free of charge via the Internet at http://pubs.acs.org.

References and Notes

(1) Boulas, P. L.; Jones, M. T.; Ruoff, R. S.; Lorents, D. C.; Malhotra, R.; Tse, D. S.; Kadish, K. M. *J. Phys. Chem.* **1996**, *100* (18), 7573–7579.

(2) Boulas, P.; Jones, M. T.; Kadish, K. M.; Ruoff, R. S.; Lorents, D. C.; Tse, D. S. *J. Am. Chem. Soc.* **1994**, *116* (20), 9393–9394.

(3) Azamar-Barrios, J. A.; Munoz, E.; Penicaud, A. *J. Chem. Soc., Faraday Trans.* **1997**, *93* (17), 3119–3123.

(4) Anderson, M. R.; Dorn, H. C.; Stevenson, S. A. *Carbon* **2000**, *38* (11−12), 1663–1670.

(5) Manolopoulos, D. E.; Fowler, P. W. *J. Chem. Phys.* **1992**, *96* (10), 7603–7614.

(6) Dennis, T. J. S.; Kai, T.; Asato, K.; Tomiyama, T.; Shinohara, H.; Yoshida, T.; Kobayashi, Y.; Ishiwatari, H.; Miyake, Y.; Kikuchi, K.; Achiba, Y. *J. Phys. Chem. A* **1999**, *103* (44), 8747–8752.

(7) Dennis, T. J. S.; Kai, T.; Tomiyama, T.; Shinohara, H. *Chem. Commun.* **1998**, (5), 619–620.

(8) Tagmatarchis, N.; Avent, A. G.; Prassides, K.; Dennis, T. J. S.; Shinohara, H. *Chem. Commun.* **1999**, (11), 1023–1024.

(9) Tagmatarchis, N.; Okada, K.; Tomiyama, T.; Yoshida, T.; Kobayashi, Y.; Shinohara, H. *Chem. Commun.* **2001**, (15), 1366–1367.

(10) Kikuchi, K.; Nakahara, N.; Wakabayashi, T.; Suzuki, S.; Shiromaru, H.; Miyake, Y.; Saito, K.; Ikemoto, I.; Kainosho, M.; Achiba, Y. *Nature* **1992**, *357* (6374), 142–145.

(11) Taylor, R.; Langley, G. J.; Avent, A. G.; Dennis, T. J. S.; Kroto, H. W.; Walton, D. R. M. *J. Chem. Soc., Perkin Trans. 2* **1993**, (6), 1029–1036.

(12) Azamar-Barrios, J. A.; Dennis, T. J. S.; Sadhukan, S.; Shinohara, H.; Scuseria, G. E.; Penicaud, A. *J. Phys. Chem. A* **2001**, *105* (19), 4627–4632.

(13) Anderson, M. R.; Dorn, H. C.; Stevenson, S. A.; Dana, S. M. *J. Electroanal. Chem.* **1998**, *444* (2), 151–154.

(14) Reed, C. A.; Bolskar, R. D. *Chem. Rev.* **2000**, *100* (3), 1075–1119.

(15) Zalibera, M.; Rapta, P.; Dunsch, L. *Electrochem. Commun.* **2008**, *10* (6), 943–946.

(16) Perdew, J. P.; Burke, K.; Ernzerhof, M. *Phys. Rev. Lett.* **1996**, *77* (18), 3865–3868.

(17) Laikov, D. N. *Chem. Phys. Lett.* **1997**, *281*, 151–156.

(18) Laikov, D. N.; Ustynyuk, Y. A. *Russ. Chem. Bull.* **2004**, *54* (3), 820–826.

(19) Barone, V. EPR-II Structure, Magnetic Properties and Reactivities of Open-Shell Species from Density Functional and Self-Consistent Hybrid Methods. In *Recent Advances in Density Functional Methods*, Part 1; Chong, D. P., Ed.; World Scientific: Singapore, 1995; p 287.

(20) Granovsky, A. A. *PC GAMESS*, Firefly version 7.1.E; http://classic.chem.msu.su/gran/gamess/index.html, 2008.

(21) Zalibera, M.; Rapta, P.; Dunsch, L. *Electrochem. Commun.* **2007**, *9* (12), 2843–2847.

(22) Dunsch, L.; Rapta, P.; Gromov, A.; Staško, A. *J. Electroanal. Chem.* **2003**, *547* (1), 35–43.

(23) Zalibera, M.; Popov, A. A.; Kalbac, M.; Rapta, P.; Dunsch, L. *Chem.—Eur. J.* **2008**, *14* (32), 9960–9967.

(24) Fukuzumi, S.; Mori, H.; Suenobu, T.; Imahori, H.; Gao, X.; Kadish, K. M. *J. Phys. Chem. A* **2000**, *104* (46), 10688–10694.

(25) Bauernschmitt, R.; Ahlrichs, R.; Hennrich, F. H.; Kappes, M. M. *J. Am. Chem. Soc.* **1998**, *120* (20), 5052–5059.

(26) Popov, A. A.; Senyavin, V. M.; Troyanov, S. I. *J. Phys. Chem. A* **2006**, *110* (23), 7414–7421.

(27) Dierksen, M.; Grimme, S. *J. Chem. Phys.* **2004**, *120* (8), 3544–3554.

JP811274G